

Synthesis and Characterization of O,N-Chelated Vanadium(IV) Oxo Phenolate Complexes: Electronic Effect of Meta and Para Substituents on the Vanadium Center

Henk Hagen,[†] Antonio Barbon,[‡] Ernst E. van Faassen,[‡] Bert T. G. Lutz,[§] Jaap Boersma,[†] Anthony L. Spek,^{||,⊥} and Gerard van Koten^{*,†}

Department of Metal-Mediated Synthesis, Debye Institute, Utrecht University, Padualaan 8, 3584 CH Utrecht, The Netherlands, Department of Atomic and Interface Physics, Debye Institute, Utrecht University, Princetonlaan 4, 3584 CC Utrecht, The Netherlands, Department of Analytical Molecular Spectrometry, Debye Institute, Utrecht University, Sorbonnelaan 16, 3584 CA Utrecht, The Netherlands, and Bijvoet Center for Biomolecular Research and Crystal and Structural Chemistry, Utrecht University, Padualaan 8, 3584 CH Utrecht, The Netherlands

Received February 8, 1999

A series of O,N-chelated vanadium(IV) oxo bis(phenolate) complexes (**1a–i**) have been prepared from [VOCl₂(THF)₂] and several ortho-amino-functionalized phenols in the presence of a base. The intermediates in the synthesis of these compounds are mono(phenolato)vanadate complexes, as was shown by the reaction of [VOCl₂(THF)₂] with 1 equiv of HOC₆H₂(CH₂NMe₂)₂-2,6-Me-4 in the absence of base. This yielded [VOCl₂(OC₆H₂(CH₂NMe₂)₂-2-Me-4-(CH₂NHMe₂)-6)] (**2**), in which the second amine function acts as an internal base, assisting in binding the formed equivalent of HCl. Complex **2** exists in the solid state as the dichlorovanadate(IV) species with the protonated amine function forming a three-centered intramolecular hydrogen bridge in which both a chloride atom and the oxygen atom of the phenolate ligand participate. EPR, UV–vis, and cyclic voltammetry analysis of the complexes with meta or para substituents (**1a–g**) on the aryloxy ring showed the hyperfine coupling constant, the HOMO–LUMO transition, and the oxidation potential, respectively, to be linearly related to the Hammett σ constants of the substituents on the monoanionic aryloxy ring. The oxidation potential shows a large dependence ($dE_{ox}/d\sigma = 170$ mV (per phenoxy ligand)) on the Hammett constant. Crystal data: **1a**, orthorhombic, *Pbca*, $a = 9.4321(7)$ Å, $b = 14.1919(14)$ Å, $c = 26.5484(14)$ Å, $V = 3553.8(5)$ Å³, $Z = 8$; **2**, monoclinic, *C2/c*, $a = 17.9977(15)$ Å, $b = 15.7445(9)$ Å, $c = 14.4986(6)$ Å, $\beta = 113.206(5)^\circ$, $V = 3776.0(4)$ Å³, $Z = 4$.

Introduction

One of the major advantages of homogeneous catalysis is the possibility of fine-tuning the catalyst by varying the ancillary ligands. In this way, chemo-, regio-, and stereoselectivity can be directed toward the desired products. One way to achieve this is by changing donor atoms in the ligands, e.g., nitrogen, phosphorus, oxygen, etc.; and a more subtle way is to change the substituents on the ligands, thereby influencing the catalytic center electronically and/or sterically.¹ In the field of catalytic α -olefin polymerization, the variation of substituents on the ligands can have large effects. Recent reports on iron-based catalysts show that, with bulky groups on the ancillary ligands, high molecular weight polyethylene is obtained.^{2,3} However,

when the steric bulk is decreased, only oligomers are formed.⁴ In neutral nickel(II) salicyldiiminato complexes, changes were visible in catalyst activity, molecular weight, and molecular weight distribution of the polymer and the number of branches upon varying the electronic influence of the ligand.⁵

We are interested in vanadium-based catalysts for the synthesis of polyolefins. By choosing the appropriate ligands, we hope to obtain well-defined ligand-controlled catalytic systems. The ligands used are monoanionic, potentially bi- or terdentate phenolate derivatives with one or two ortho-amine functions (see Figure 1). For the system VCl₂(OR)₂ (OR = **a**), we have found high catalyst stability and activity in ethene polymerization.⁶

These ligands have a great potential for tuning both steric and electron influences. Variation of substituents at the ortho position on the ring and on the nitrogen-donor atom, which are both close to the reactive center, will result in both steric and electronic changes. To isolate the electronic from any steric influence, the substituents have to be situated at the meta or para positions relative to the metal center, in which case they can exert mesomeric and/or inductive effects. To study these effects of ring substitution on the metal center we have prepared a series of vanadyl bis(phenolates) ([V^{IV}(=O)(OR)₂], OR = **a–g**). These paramagnetic d¹ compounds were analyzed with

* To whom correspondence should be addressed. E-mail: g.vankoten@chem.uu.nl.

[†] Department of Metal-Mediated Synthesis.

[‡] Department of Atomic and Interface Physics.

[§] Department of Analytical Molecular Spectrometry.

^{||} Bijvoet Center for Biomolecular Research and Crystal and Structural Chemistry.

[⊥] To whom correspondence pertaining to crystallographic studies should be addressed. E-mail: a.l.spek@chem.uu.nl.

(1) van Leeuwen, P. W. N. M.; van Koten, G. In *Catalysis: An Integrated Approach to Homogeneous, Heterogeneous and Industrial Catalysis*; Mouljijn, J. A., van Leeuwen, P. W. N. M., van Santen, R. A., Eds.; Elsevier: Amsterdam, 1993; Chapter 6.

(2) Britovsek, G. J. P.; Gibson, V. C.; Kimberley, B. S.; Maddox, P. J.; McTavish, S. J.; Solan, G. A.; White, A. J. P.; Williams, D. J. *Chem. Commun.* **1998**, 849.

(3) Small, B. L.; Brookhart, M.; Bennett, A. M. A. *J. Am. Chem. Soc.* **1998**, *120*, 4049.

(4) Small, B. L.; Brookhart, M. *J. Am. Chem. Soc.* **1998**, *120*, 7143.

(5) Wang, C.; Friedrich, S.; Younkin, T. R.; Li, R. T.; Grubbs, R. H.; Bansleben, D. A.; Day, M. W. *Organometallics* **1998**, *17*, 3149.

(6) Hagen, H.; et al. To be published.

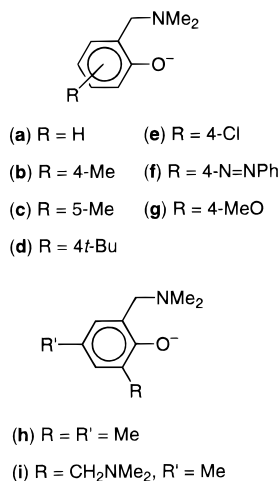


Figure 1. Selected monoanionic phenol derivatives.

EPR spectroscopy, UV-vis spectroscopy, and cyclic voltammetry. We have chosen these vanadyl compounds instead of the actual vanadium(IV) dichloro catalysts, [VOCl₂(OR)₂], for studying the influence of the phenolate ligands because they are more stable toward air while the d-d transitions in the UV-vis region are not masked by charge-transfer bands, as is the case for vanadium(IV) dichloro species.⁷

Experimental Section

General Procedures. All reactions were performed in an atmosphere of dry, oxygen-free dinitrogen using standard Schlenk techniques. All solvents were carefully dried and distilled prior to use. [VOCl₂(THF)₂]⁸ and the phenols (**a-e**, **g-i**)⁹ were prepared according to literature procedures. The sodium phenolate NaOC₆H₄(CH₂NMe₂)-2 was prepared by treating the corresponding phenol with NaH in hexane.¹⁰ Et₃N was distilled from CaH₂. All other chemicals were obtained from commercial sources and used as received. Elemental analyses were performed by H. Kolbe, Mikroanalytisches Laboratorium, Mülheim, Germany. ¹H NMR spectra were recorded on a Bruker AC300 spectrometer, and UV-vis spectra were recorded on a Cary 1 or a Cary 5 UV-vis spectrophotometer. Differential scanning calorimetry was done using a Mettler DSC 12E with the samples in sealed aluminum pans (heating rate 5 °C/min). Thermogravimetry was performed on a Perkin-Elmer TGS-2 thermogravimetric system under a nitrogen atmosphere (heating rate 20 °C/min).

EPR Spectroscopy. The experiments were carried out at room temperature on a Bruker ESP300 spectrometer, equipped with a Bruker ST1 cavity (operating in the TE₁₀₂ mode with unloaded $Q = 3800$). The sample solutions were enclosed in sealed quartz tubes ($\varnothing = 2$ mm), which were then placed inside a standard Bruker quartz dewar used for temperature control via a N₂ flow thermostat (Bruker ER 4111 VT, temperature stability 1 K). In this setup, a total of 80 mm³ of sample liquid is inside the cavity, adequate for good S/N ratios. The concentrations were in the 2–5 mM range. The magnetic field was centered at 3400 G, with a sweep width of 1000 G. The magnetic field was modulated with a frequency of 100 Hz and an amplitude of 0.5 G. The spectra contain 8K points, resulting in good field resolution.

Synthesis of HOC₆H₄(CH₂NMe₂)-2-(N=NPh)-4 (f). To a mixture of aniline (6.42 g, 68.4 mmol) and HCl (25 mL, 10 M) in water (150 mL) was added NaNO₂ (5.40 g, 78.2 mmol) in water (30 mL) at 0 °C in 15 min. The resulting yellowish solution was stirred for 15 min. After this period, the solution was added to a mixture of HOC₆H₄(CH₂-

NMe₂)-2 (**a**) (9.32 g, 61.6 mmol) and NaOAc (15.8 g, 0.19 mol) in a water/ice mixture (250 mL) during 1 h while the temperature was maintained at 0 °C. The solution immediately turned yellow and eventually dark red. After all of the diazonium salt had been added, the clear red solution was stirred for 1 h and was allowed to warm to room temperature. The solution was then neutralized by adding solid NaHCO₃ and extracted with Et₂O (150/75 mL). The ethereal solutions were combined and washed with a saturated NaCl solution (3 × 50 mL). After the mixture was dried with MgSO₄, the solvent was removed in vacuo, leaving a dark red oil, which solidified upon standing. Sublimation (100 °C, 0.1 mmHg) gave analytically pure, bright orange crystals. Mp: 79 °C. Anal. Calcd for C₁₅H₁₇N₃O: C, 70.56; H, 6.71; N, 16.46. Found: C, 70.49; H, 6.81; N, 16.39. ¹H NMR (CDCl₃, 300 MHz): δ 2.38 (s, 6 H, NMe₂), 3.76 (2 H, s, CH₂), 6.95 (d, 1 H, ³J_{H,H} = 8.6 Hz, Ar H), 7.5 (m, 3 H, Ar H), 7.64 (d, 1 H, ⁴J_{H,H} = 2.3 Hz, Ar H), 7.8 (m, 3 H, Ar H), 10.56 (br, 1 H, OH). UV-vis (H₂O; λ_{\max} (nm), ϵ (M⁻¹ cm⁻¹)): 395, 1.7 × 10⁴; 269, 6.1 × 10³; 246, 6.2 × 10³; 193, 2.4 × 10⁴.

Synthesis of [VO(OC₆H₄(CH₂NMe₂)-2)₂] (1a). **(a) From the Sodium Phenolate.** To a solution of [VOCl₂(THF)₂] (0.96 g, 3.4 mmol) in THF (30 mL) was added dropwise a solution of Na(OC₆H₄(CH₂-NMe₂)-2) (1.17 g, 6.8 mmol) in THF (30 mL) at -15 °C. A very dark solution was obtained which turned into a reddish suspension upon warming to room temperature. The suspension was stirred for 16 h. The blue/purple supernate was isolated by centrifugation/decantation, and the solvent was removed in vacuo to yield a dark blue solid (1.10 g). This solid was extracted with Et₂O. The ethereal extract was concentrated in vacuo to 15 mL and cooled to -20 °C to yield dark blue crystals (0.69 g, 55%). Mp: 161 °C. Anal. Calcd for C₁₈H₂₄N₂O₅V: C, 58.85; H, 6.59; N, 7.63. Found: C, 58.66; H, 6.54; N, 7.57. UV-vis (hexane; λ_{\max} (nm), ϵ (M⁻¹ cm⁻¹)): 839, 69; 535, 50; 395, 3.1 × 10⁴; 253, 1.3 × 10⁴. (toluene; λ_{\max} (nm), ϵ (M⁻¹ cm⁻¹)): 877, 59; 541, 42; 397, 26. EPR (hexane): $A_{\text{iso}} = 101.5$ G, $g_{\text{iso}} = 1.9719$. EPR (toluene): $A_{\text{iso}} = 100.65$ G, $g_{\text{iso}} = 1.9714$.

(b) From the Phenol. To a mixture of HOC₆H₄(CH₂NMe₂)-2 (**a**) (1.21 g, 8.0 mmol) and Et₃N (1.5 mL, excess) in Et₂O (25 mL) was added a solution of [VOCl₂(THF)₂] (1.14 g, 4.0 mmol) in Et₂O (60 mL). During the addition, the solution turned purple while a white precipitate was formed. The resulting mixture was stirred for 1 h, and the precipitate was removed by centrifugation. Removal of the solvent of the supernate in vacuo gave a blue solid (1.22 g, 83%).

Synthesis of [VO(OC₆H₃(CH₂NMe₂)-2-Me-4)₂] (1b). To a mixture of HOC₆H₃(CH₂NMe₂)-2-Me-4 (**b**) (1.46 g, 8.8 mmol) and Et₃N (3 mL, excess) in Et₂O (10 mL) was added a solution of [VOCl₂(THF)₂] (1.27 g, 4.5 mmol) in Et₂O (75 mL). The solution turned purple while a white precipitate was formed. The resulting mixture was stirred for 16 h, and the precipitate was removed by centrifugation. Removal of the solvent of the supernate in vacuo gave a blue oil (1.40 g). When the blue oil was dissolved in pentane and the solution was cooled to -25 °C, a blue crystalline material was formed (0.98 g, 55%). Analytically pure needle-shaped crystals were obtained by crystallization from MeNO₂. Mp: 124 °C. Anal. Calcd for C₂₀H₂₈N₂O₅V: C, 60.75; H, 7.14; N, 7.09. Found: C, 60.81; H, 7.15; N, 7.18. UV-vis (toluene; λ_{\max} (nm), ϵ (M⁻¹ cm⁻¹)): 882, 65; 540, 47; 398, 32. EPR (toluene, 3.5 mM): $A_{\text{iso}} = 100.42$ G, $g_{\text{iso}} = 1.9714$.

Synthesis of [VO(OC₆H₃(CH₂NMe₂)-2-Me-5)₂] (1c). To a mixture of HOC₆H₃(CH₂NMe₂)-2-Me-5 (**c**) (1.78 g, 10.8 mmol) and Et₃N (3 mL, excess) in Et₂O (10 mL) was added a solution of [VOCl₂(THF)₂] (1.49 g, 5.3 mmol) in Et₂O (75 mL). The resulting mixture was stirred for 16 h, and the pale pink supernate was decanted. The purple residue was washed with MeOH (2 × 10 mL) and dried in vacuo, yielding a blue/purple powder (1.62 g, 77%). Recrystallization from boiling toluene gave analytically pure, blue crystals. Mp: 255 °C dec. Anal. Calcd for C₂₀H₂₈N₂O₅V: C, 60.75; H, 7.14; N, 7.09. Found: C, 60.73; H, 7.43; N, 6.98. UV-vis (toluene; λ_{\max} (nm), ϵ (M⁻¹ cm⁻¹)): 887, 61; 541, 44; 397, 28. EPR (toluene, 2.2 mM): $A_{\text{iso}} = 100.52$ G, $g_{\text{iso}} = 1.9715$.

Synthesis of [VO(OC₆H₃(CH₂NMe₂)-2-*t*-Bu-4)₂] (1d). To a mixture of HOC₆H₃(CH₂NMe₂)-2-*t*-Bu-4 (**d**) (2.71 g, 13.1 mmol) and Et₃N (5 mL, excess) in Et₂O (10 mL) was added a solution of [VOCl₂(THF)₂] (1.87 g, 6.6 mmol) in Et₂O (70 mL). During the addition, the solution

(7) Jezierski, A.; Raynor, J. B. *J. Chem. Soc., Dalton Trans.* **1981**, 1.
 (8) Kern, R. *J. Inorg. Nucl. Chem.* **1962**, *24*, 1105.
 (9) *Methoden der Organische Chemie*, 4th ed.; Houben, J.; Weyl, T., Eds.; Georg Thieme Verlag: Stuttgart, Germany, 1957; Vol. 11/1; p 756.
 (10) van der Schaaf, P. A.; Jastrzebski, J. T. B. H.; Hogerheide, M. P.; Smeets, W. J. J.; Spek, A. L.; van Koten, G. *Inorg. Chem.* **1993**, *32*, 4111.

turned purple while a white precipitate was formed. The resulting mixture was stirred for 1 h, and the precipitate was removed by centrifugation. Removal of the solvent of the supernate in vacuo gave a blue oil (2.45 g). The compound solidified upon the addition of pentane (50 mL). After the volume of the supernate had been reduced in vacuo to 10 mL, the supernate was decanted. The residue was dried in vacuo, yielding a blue powder (1.88 g, 59%). Recrystallization from MeNO₂ (60 mL) at 13 °C yielded blue crystals. Mp: 188 °C. Anal. Calcd for C₂₆H₄₀N₂O₃V: C, 65.12; H, 8.41; N, 5.84. Found: C, 64.97; H, 8.56; N, 5.91. UV-vis (hexane; λ_{max} (nm), ε (M⁻¹ cm⁻¹)): 873, 71; 534, 53; 394, 37; 254, 2.4 × 10⁴; 209, 4.9 × 10⁴. UV-vis (*i*-PrOH; λ_{max} (nm), ε (M⁻¹ cm⁻¹)): 920, 54; 606, 40; 551, 42; 257, 9.9 × 10³; 205, 3.8 × 10⁴. UV-vis (toluene, λ_{max} (nm), ε (M⁻¹ cm⁻¹)): 883, 63; 539, 47; 397, 31. EPR (hexane): A_{iso} = 101.2 G, g_{iso} = 1.9702. EPR (toluene, 4.5 mM): A_{iso} = 100.24 G, g_{iso} = 1.9717.

Synthesis of [VO(OC₆H₃(CH₂NMe₂)-2-Cl-4)₂] (1e). To a mixture of HOC₆H₃(CH₂NMe₂)-2-Cl-4 (e) (2.01 g, 10.8 mmol) and Et₃N (3 mL, excess) in Et₂O (10 mL) was added a solution of [VOCl₂(THF)₂] (1.57 g, 5.6 mmol) in Et₂O (60 mL). The solution turned purple while a white precipitate was formed. The resulting mixture was stirred for 16 h, and the precipitate was removed by centrifugation. The residue was extracted with Et₂O (3 × 40 mL). When the combined ethereal fractions were cooled to -25 °C, blue crystals were formed (0.79 g, 33%). Mp: 208 °C. Anal. Calcd for C₂₀H₂₂N₂O₃VCl₂: C, 49.56; H, 5.08; N, 6.42. Found: C, 49.73; H, 5.16; N, 6.50. UV-vis (toluene; λ_{max} (nm), ε (M⁻¹ cm⁻¹)): 867, 65; 540, 49; 396, 30. EPR (toluene, 2.6 mM): A_{iso} = 100.74 G, g_{iso} = 1.9720.

Synthesis of [VO(OC₆H₃(CH₂NMe₂)-2-(N=NPh)-4)₂] (1f). To a mixture of HOC₆H₄(CH₂NMe₂)-2-(N=NPh)-4 (f) (2.82 g, 12.5 mmol) and Et₃N (4 mL, excess) in Et₂O (15 mL) was added a solution of [VOCl₂(THF)₂] (1.76 g, 6.2 mmol) in Et₂O (60 mL). The solution turned red while a white precipitate was formed. The resulting mixture was stirred for 16 h. After removal of the solvent in vacuo, the residue was extracted with toluene (2 × 40 mL). The volume of the combined fractions was reduced to 40 mL in vacuo. Addition of pentane (40 mL) and cooling to -20 °C gave dark red crystals in two crops (1.80 and 0.73 g). These crystals contained approximately 1 equiv of toluene, of which 50% could be removed by heating at 80 °C in vacuo. Mp: 148 °C. Anal. Calcd for C₃₀H₃₂N₆O₃V·C₇H₈: C, 64.38; H, 5.89; N, 13.65. Found: C, 64.94; H, 5.82; N, 13.49. UV-vis (toluene; λ_{max} (nm), ε (M⁻¹ cm⁻¹)): 856, 105; 382, 4.0 × 10⁴. EPR (toluene, 3.1 mM): A_{iso} = 100.95 G, g_{iso} = 1.9721.

Synthesis of [VO(OC₆H₃(CH₂NMe₂)-2-OMe-4)₂] (1g). To a mixture of HOC₆H₃(CH₂NMe₂)-2-OMe-4 (g) (1.56 g, 8.6 mmol) and Et₃N (3 mL, excess) in Et₂O (10 mL) was added a solution of [VOCl₂(THF)₂] (1.21 g, 4.3 mmol) in Et₂O (30 mL). During the addition, a grayish green suspension was formed. The solution turned purple slowly while a white precipitate was formed. The resulting mixture was stirred for 16 h, and the precipitate was removed by centrifugation. The residue was extracted with Et₂O (2 × 40 mL). The volume of the combined ethereal fractions was reduced to 100 mL in vacuo. Cooling the solution to -25 °C yielded blue crystals (0.64 g, 35%). Mp: 169 °C. Anal. Calcd for C₂₀H₂₈N₂O₅V: C, 56.21; H, 6.60; N, 6.55. Found: C, 56.35; H, 6.74; N, 6.48. UV-vis (toluene; λ_{max} (nm), ε (M⁻¹ cm⁻¹)): 886, 65; 538, 32. EPR (toluene, 4.8 mM): A_{iso} = 100.25 G, g_{iso} = 1.9714.

Synthesis of [VO(OC₆H₂(CH₂NMe₂)-2-Me₂-4,6)₂] (1h). To a mixture of HOC₆H₂(CH₂NMe₂)-2-Me₂-4,6 (h) (1.44 g, 8.0 mmol) and Et₃N (2 mL, excess) in Et₂O (10 mL) was added a solution of [VOCl₂(THF)₂] (1.15 g, 4.1 mmol) in Et₂O (60 mL). During the addition, the solution turned purple while a white precipitate was formed. The resulting mixture was stirred for 1 h, and the solvent was removed in vacuo. The resulting purple solid was extracted with benzene (3 × 40 mL). Upon combination of the three extracts and removal of the solvent in vacuo, VO(OC₆H₂(CH₂NMe₂)-2-Me₂-4,6)₂ was obtained as a pale purple solid (1.75 g, 89%). Recrystallization from MeNO₂ yielded blue crystals. Mp: 213 °C. Anal. Calcd for C₂₂H₃₂N₂O₃V: C, 62.40; H, 7.62; N, 6.62. Found: C, 62.54; H, 7.65; N, 6.75. UV-vis (hexane; λ_{max} (nm), ε (M⁻¹ cm⁻¹)): 884, 72; 540, 54; 258, 1.8 × 10⁴; 209, 5.4 × 10⁴. EPR (hexane): A_{iso} = 100.8 G, g_{iso} = 1.9722.

Synthesis of [VO(OC₆H₂(CH₂NMe₂)-2,6-Me-4)₂] (1i). Addition of [VOCl₂(THF)₂] (1.13 g, 4.0 mmol) in Et₂O (60 mL) to a mixture of

Table 1. Crystal Data for 1a and 2

	1a	2
formula	C ₁₈ H ₂₄ N ₂ O ₃ V	C ₁₃ H ₂₂ Cl ₂ N ₂ O ₂ V·1/2CH ₂ Cl ₂
MW	367.33	805.29
space group	<i>Pbca</i> (No. 61)	<i>C2/c</i> (No. 15)
crystal system	orthorhombic	monoclinic
Z	8	4
<i>a</i> , Å	9.4321(7)	17.9977(15)
<i>b</i> , Å	14.1919(14)	15.7445(9)
<i>c</i> , Å	26.5484(14)	14.4986(6)
β, deg		113.206(5)
<i>V</i> , Å ³	3553.8(5)	3776.0(4)
<i>D</i> _{calc} , g·cm ⁻³	1.373	1.416
μ(Mo Kα), mm ⁻¹	0.6	0.96
final R ^a	0.0565	0.0416
final wR ^b	0.1049	0.1104
GoF	0.97	1.03

$$^a R = \sum(|F_o| - |F_c|) / \sum|F_o|. \quad ^b wR_2 = [\sum w(F_o^2 - F_c^2)^2 / \sum w(F_o^2)^2]^{1/2}.$$

HOC₆H₂(CH₂NMe₂)-2,6-Me-4 (i) (1.73 g, 7.8 mmol) and Et₃N (3 mL, excess) in Et₂O (20 mL) gave a blue/purple solution with a white precipitate. Removal of the solvent in vacuo yielded a blue sticky solid. Extraction of this solid with pentane (2 × 30 mL) and subsequent removal of the solvent in vacuo afforded a blue oil (2.00 g, 98%). Crystallization of this oil from MeNO₂ at 0 °C gave blue crystals. These crystals contained approximately 1 equivalent of MeNO₂, which could be removed by heating overnight at 110 °C in vacuo. Mp: 136 °C. Anal. Calcd for C₂₆H₄₂N₄O₃V: C, 61.28; H, 8.31; N, 10.99. Found: C, 61.32; H, 8.28; N, 10.97. UV-vis (hexane; λ_{max} (nm), ε (M⁻¹ cm⁻¹)): 885, 7.27 × 10³; 542, 5.58 × 10³; 259, 1.60 × 10⁴. EPR (hexane): A_{iso} = 100.5 G, g_{iso} = 1.9722.

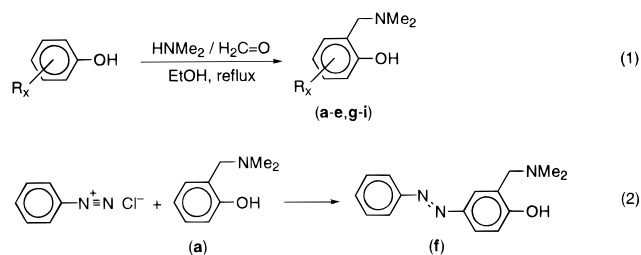
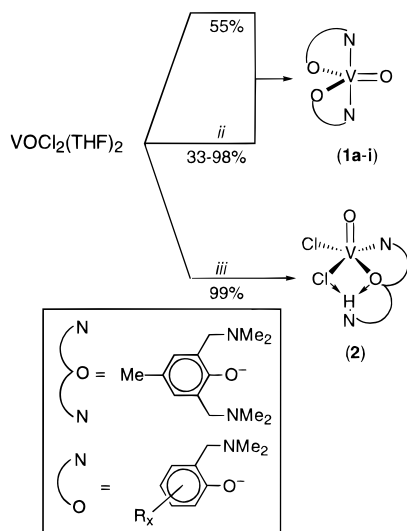
Synthesis of [VOCl₂(OC₆H₂(CH₂NMe₂)-2-Me-4-(CH₂NHMe₂)-6)₂] (2). To a solution of [VOCl₂(THF)₂] (0.89 g, 3.2 mmol) in Et₂O (40 mL) was added dropwise a solution of HOC₆H₂(CH₂NMe₂)-2,6-Me-4 (i) (0.68 g, 3.1 mmol) in Et₂O (15 mL). Immediately a green suspension was formed. After 1 h of stirring, the supernate was decanted. Washing of the precipitate with Et₂O (20 mL) and subsequent drying in vacuo afforded a pale blue/green powder (1.13 g, 99%). Recrystallization from CH₂Cl₂ gave blue crystals. Anal. Calcd for C₁₃H₂₂N₂O₂Cl₂V·0.5CH₂Cl₂: C, 39.37; H, 5.85; N, 7.06. Found: C, 39.20; H, 5.75; N, 6.78. UV-vis (CH₂Cl₂; λ_{max} (nm), ε (M⁻¹ cm⁻¹)): 755, 41; 610, 23; 409, 13; 291, 3.24 × 10³; 240, 4.57 × 10³. EPR (CH₂Cl₂): A_{iso} = 103.4 G, g_{iso} = 1.9719

X-ray Crystallographic Determinations and Refinements. Dark blue crystals of 1a suitable for X-ray diffraction were grown from Et₂O at -20 °C while pale blue crystals of 2·0.5CH₂Cl₂ were grown from CH₂Cl₂ at room temperature. X-ray data were collected on an Enraf-Nonius CAD4T (rotating anode) diffractometer at 150 K (Mo Kα) for 1a and 225 K for 2 for cut-to-size, inert oil covered, crystals. Compound 2 has a phase transition to a triclinic structure between 225 and 150 K. The data for the low-temperature phase have been deposited with the Cambridge Structural Database (CCDC 106615).

Both structures were solved with DIRDIF/PATY¹¹ and refined on F² with SHELXL96.¹² The intensity data were corrected for absorption with the empirical PLATON/DELABS¹³ procedure for 1a or with the analytical de Meulenaer and Tompa¹⁴ correction method (PLATON/ABST)¹³ for 2. The position of H1 in 2 was found in a difference density Fourier map at bonding distance to N2, but its position was not refined.

Relevant numerical data have been collected in Table 1. Geometrical calculations and the ORTEP illustration were done with PLATON.¹³

- Beurkens, P. T.; Admiraal, G.; Beurskens, G.; Bosman, W. P.; García-Granda, S.; Gould, R. O.; Smits, J. M. M.; Smykalla, C. *The DIRDIF96 Program System*; Technical Report of the Crystallographic Laboratory, University of Nijmegen: Nijmegen, The Netherlands, 1992.
- Sheldrick, G. M. *SHELXL-96: Program for Crystal Structure Refinement*; University of Göttingen: Göttingen, Germany, 1996.
- Spek, A. L. *Acta Crystallogr.* **1990**, *A46*, C-34.
- de Meulenaer, J.; Tompa, H. *Acta Crystallogr.* **1965**, *19*, 1014.

Scheme 1. Synthesis of Ligands **a–g****Scheme 2**^a

^a Key: (i) 2 equiv of $\text{NaOC}_6\text{H}_4(\text{CH}_2\text{NMe}_2)_2$, THF, $-15\text{ }^\circ\text{C}$; (ii) 2 equiv of HOR (**a–i**) and 50–100% excess of Et_3N , Et_2O , RT; (iii) 1 equiv of $\text{HOC}_6\text{H}_2(\text{CH}_2\text{NMe}_2)_2$ -2,6-Me-4, Et_2O , RT.

Results and Discussion

Synthesis. The phenols **a–e** and **g–i** were prepared from the corresponding phenols by a Mannich reaction with dimethylamine and formaldehyde in ethanol (Scheme 1(1)).⁹ For compounds with strong electron-withdrawing groups, like CF_3 , this reaction is very slow, and during the long reaction time required, a mixture of unidentified products is formed. To obtain a phenol with a strong electron-withdrawing group on the ring, the Mannich base has to be prepared prior to functionalization, which can then be carried out by an electrophilic aromatic substitution.¹⁵ The azo-substituted phenol (**f**) was thus prepared in a diazonium coupling reaction of benzenediazonium chloride and **a** (Scheme 1(2)).

Initially, $[\text{VO}(\text{OC}_6\text{H}_4(\text{CH}_2\text{NMe}_2)_2)_2]$ (**1a**) was prepared by reacting $[\text{VOCl}_2(\text{THF})_2]$ with the corresponding sodium phenolate (Scheme 2(i)). However a more convenient route was found when $[\text{VOCl}_2(\text{THF})_2]$ was reacted with the phenol in the presence of Et_3N as a base (Scheme 2(ii)). In this way, several bis(phenolates) (**1a–h**) were prepared in high yields. These reactions proceed instantaneously at room temperature.

The solubility of the vanadyl bis(phenolates) is very much influenced by the substituents. All compounds except **1c** and **1h** are quite soluble in aromatics, Et_2O , CH_2Cl_2 , THF, and MeNO_2 . Compounds **1b**, **1d**, and **1i** are also quite soluble in pentane and hexane. In contrast, **1h** is only slightly soluble in aromatics and polar solvents such as CH_2Cl_2 , THF, and MeNO_2 while **1c** is poorly soluble only in aromatics.

These compounds melt without decomposition with a melting temperature range of $124\text{ }^\circ\text{C}$ (**1b**) to $213\text{ }^\circ\text{C}$ (**1h**). Only **1c** decomposes on melting at $255\text{ }^\circ\text{C}$.

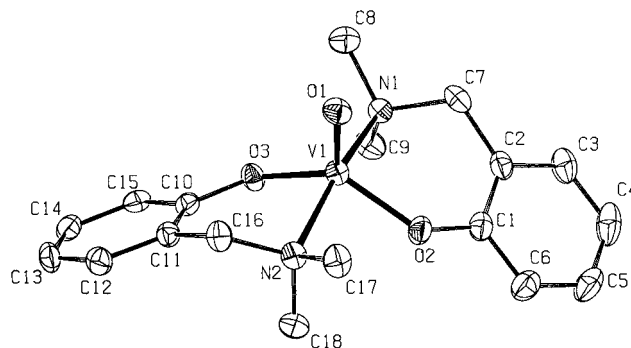


Figure 2. Molecular structure of **1a**. Hydrogen atoms are omitted for clarity.

Whereas in the solid state these compounds are stable in air at least for some hours, in solution they decompose readily when in contact with air.

In the reactions of $[\text{VOCl}_2(\text{THF})_2]$ with the phenols in the presence of Et_3N as a base, it was noticed that, upon the addition of the first equivalent of the phenol, a very insoluble pale green material was formed quantitatively. Addition of the second equivalent resulted in the formation of the desired bis(phenolates). Due to the insolubility of the green compound, we were not able to determine its exact nature, but on the basis of the mass balance, we concluded in the case of $\text{HOC}_6\text{H}_4(\text{CH}_2\text{NMe}_2)_2$ (**a**) that this insoluble material had to be the vanadate(IV) salt $[\text{Et}_3\text{NH}][\text{VOCl}_2(\text{OR})\cdot\text{THF}]$. This conclusion was indirectly supported by the results of the experiments of the bis(amino)phenol **i** with $[\text{VOCl}_2(\text{THF})_2]$. When the reaction was carried out in the absence of base (Scheme 2(iii)), a green compound with the stoichiometry $[\text{VOCl}_2(\text{OC}_6\text{H}_2(\text{CH}_2\text{NMe}_2)_2\text{-Me-4-(CH}_2\text{NHMe}_2)_6)]$ (**2**) was formed quantitatively; i.e., in this case, the second amino substituent functions as an internal base and is converted into an ammonium substituent. Compound **2** is completely insoluble in apolar solvents such as pentane, hexane, and aromatics as well as in Et_2O , but it is slightly soluble in THF and dissolves readily in CH_2Cl_2 and pyridine.

Compound **2** is stable in air for hours and is also thermally very stable. Thermal gravimetric analysis (TGA) of **2** shows a small decrease in weight starting at $170\text{ }^\circ\text{C}$. This is attributed to the escape of CH_2Cl_2 , which is accompanied by destruction of the crystal lattice with retention of the color. Between 210 and $238\text{ }^\circ\text{C}$, there is a sharp well-defined decrease in weight of 9.1%. With a molecular weight of 402.65,¹⁶ this implies the removal of a compound with a molecular weight of 36.6, which agrees nicely with the removal of 1 equiv of HCl (MW = 36.5). The removal of HCl is accompanied by a color change from pale greenish blue to dark green.

Structures of 1a and 2 in the Solid State. Due to the paramagnetism of the d^1 vanadium(IV) complexes, no structural information can be obtained with NMR, and a single-crystal X-ray structure determination is therefore of great importance. Crystallization of **1a** from Et_2O gave single crystals suitable for X-ray structure analysis. The molecular structure of **1a** is depicted in Figure 2. Selected bond lengths and angles are given in Table 2.

The geometry around the vanadium center is a distorted trigonal bipyramid (37% on the Berry pseudorotation path between D_{3h} and C_{4v}). The three oxygen atoms are in the

(15) McMurry, J. *Organic Chemistry*, 2nd ed.; Brooks/Cole Publishing Co.: Pacific Grove, CA, 1988.

(16) Crystals of **2** contain 0.5 equiv of CH_2Cl_2 . Anal. Calcd for $\text{C}_{13}\text{H}_{22}\text{N}_2\text{O}_2\text{-Cl}_2\text{V}\cdot 0.5\text{CH}_2\text{Cl}_2$: C, 39.37; H, 5.85; N, 7.06. Found: C, 39.20; H, 5.75; N, 6.78.

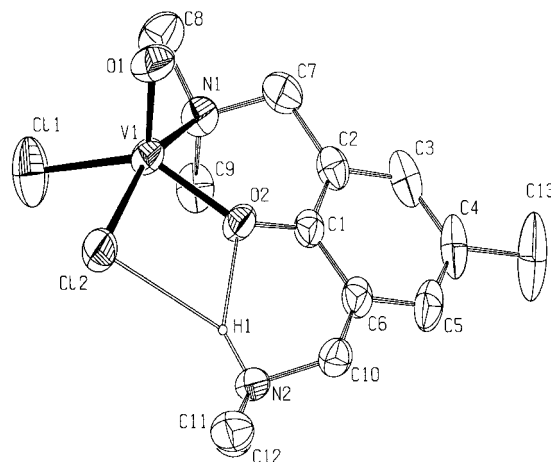
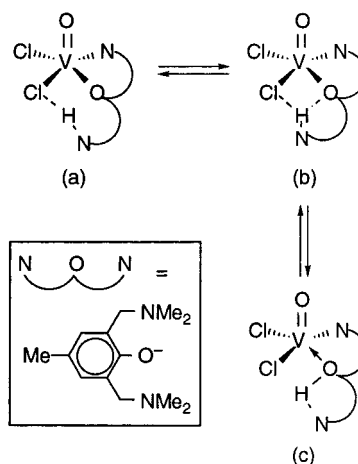
Table 2. Selected Bond Lengths and Bond Angles for **1a** and **2**

	1a	2
Bond Lengths (Å)		
V1–O1	1.599(2)	1.5803(19)
V1–O2	1.897(2)	1.9065(19)
V1–O3	1.883(2)	
V1–N1	2.155(3)	2.157(2)
V1–N2	2.147(3)	
V1–C11		2.3096(11)
V1–C12		2.3946(8)
O2–C1	1.342(4)	1.341(3)
O3–C10	1.348(4)	
Bond Angles (deg)		
O1–V1–O2	115.84(11)	110.37(10)
O1–V1–O3	114.12(11)	
O2–V1–O3	130.02(10)	
V1–O2–C1	133.6(2)	135.84(16)
V1–O3–C10	133.52(19)	
O1–V1–N1	97.71(13)	96.37(9)
O1–V1–N2	97.16(12)	
N1–V1–N2	165.13(11)	
O2–V1–N1	88.44(11)	86.37(8)
O3–V1–N2	87.59(10)	
O1–V1–C11		110.65(9)
O1–V1–C12		102.91(8)
N1–V1–C11		89.65(7)
C11–V1–C12		88.65(3)
C12–V1–O2		81.88(5)

equatorial plane ($\Sigma(\text{O}-\text{V}-\text{O}) = 359.98(2)^\circ$) while the two coordinating nitrogen atoms are in the apical positions ($\text{N1}-\text{V}-\text{N2} = 165.13(11)^\circ$); i.e., both O,N-bidentately bonded phenolate ligands are bound to the vanadium in a similar way. While five-coordinated vanadium complexes generally adopt square pyramidal geometries, the presence of steric bulk on the coordinating nitrogen atoms causes the distortion toward a trigonal bipyramidal geometry. This conclusion is corroborated by what was recently shown for vanadyl complexes with sterically crowded Schiff base ligands.¹⁷ The $\text{V}=\text{O}$ (1.599(2) Å) and the $\text{V}-\text{O}$ distances (average 1.890(2) Å) are in the ranges normally found for vanadyl phenolates (1.57–1.68 Å¹⁸ and 1.811(7)–1.990(9) Å,^{19,20} respectively).

Crystallization of **2** from CH_2Cl_2 gave single crystals suitable for X-ray structure analysis. The molecular structure of **2** (see Figure 3 and Table 2) establishes that **2** is a vanadate complex with a five-coordinated distorted square pyramidal geometry (61% on the Berry pseudorotation path between D_{3h} and C_{4v}) for the vanadium center. The basal plane is formed by the two chloride anions Cl1 and Cl2, the oxygen of the phenolate O2, and a coordinating amine substituent N1 of the phenolate ligand. The oxygen atom O1 is in the apical position of the square pyramid. The vanadium atom is at a distance of 0.556(0) Å above the basal plane. The second amine function N2 is quaternized with the $\text{N2}-\text{H1}$ vector pointing in the direction of both O2 and Cl2. The $\text{V}-\text{N}$ and $\text{V}=\text{O}$ bond lengths in **2** are similar to those in the bis(phenolate) complex **1a**.

For the neutral phenol ligand, three H-bonding forms can be envisaged (see Figure 4). In bonding mode a, the phenol is present as an anionic ligand with a proton solely bound to the nitrogen atom; cf. the lanthanum and yttrium complexes [Ln-

**Figure 3.** Molecular structure of **2**. Other hydrogen atoms are omitted for clarity.**Figure 4.** Possible H-bonding forms of **2**.

$[\text{OC}_6\text{H}_2(\text{CH}_2\text{NMe}_2)_2-2,6-\text{Me}-4]_3(\text{OC}_6\text{H}_2(\text{CH}_2\text{N}(\text{H})\text{Me}_2)-2-(\text{CH}_2-\text{NMe}_2)-6-\text{M}-4)]$ (Ln = La, Y).²¹ In **2**, this would imply that a hydrogen bridge is present between the nitrogen and one of the chloride ions, something which is well-documented for metal chlorides.²² In bonding mode c, the phenol is present as a neutral ligand. The hydrogen is positioned on the oxygen, and a hydrogen bridge is formed between the oxygen atom and the noncoordinating nitrogen atom. Thus, the phenol is coordinated in an ethereal motif (mode c); cf. the bonding in the sodium phenolate complex $[(\text{NaOC}_6\text{H}_2(\text{CH}_2\text{NMe}_2)_2-2,6-\text{Me}-4)(\text{HOC}_6\text{H}_2(\text{CH}_2\text{NMe}_2)_2-2,6-\text{Me}-4)]_2$.²³ An intermediate bonding mode (mode b) comprises a proton–oxygen interaction as well as a proton–halide interaction.

To describe the bonding mode in **2** best, the bond lengths from the hydrogen atom to the acceptor atoms have to be considered. The $\text{H1}-\text{O2}$ and $\text{H1}-\text{Cl2}$ distances of 1.87 and 2.51 Å, respectively, are both considerably shorter than the combined van der Waals radii (2.72 and 2.90 Å). This means that hydrogen bonds are present between both the oxygen and the chlorine atoms; i.e., bonding mode b is present in **2**. A three-centered or bifurcated configuration implies that the hydrogen

(17) Cornman, C. R.; Geiser-Bush, K. M.; Rowley, S. P.; Boyle, P. D. *Inorg. Chem.* **1997**, *36*, 6401.

(18) Clark, R. J. H. In *Comprehensive Inorganic Chemistry*; Trotman-Dickenson, A. F., Ed.; Pergamon Press: Oxford, U.K., 1973; Vol. 3, p 514.

(19) Oyaizu, K.; Yamamoto, K.; Yoneda, K.; Tsuchida, E. *Inorg. Chem.* **1996**, *35*, 6634.

(20) Mohanta, S.; Nanda, K. K.; Ghosh, S.; Mukherjee, M.; Helliwell, M.; Nag, K. *J. Chem. Soc., Dalton Trans.* **1996**, 4233.

(21) Hogerheide, M. P.; Ringelberg, S. N.; Jastrzebski, J. T. B. H.; Boersma, J.; Spek, A. L.; van Koten, G. To be published.

(22) Aullón, G.; Bellamy, D.; Brammer, L.; Bruton, E. A.; Orpen, A. G. *Chem. Commun.* **1998**, 653.

(23) Hogerheide, M. P.; Ringelberg, S. N.; Janssen, M. D.; Boersma, J.; Spek, A. L.; van Koten, G. *Inorg. Chem.* **1996**, *35*, 1195.

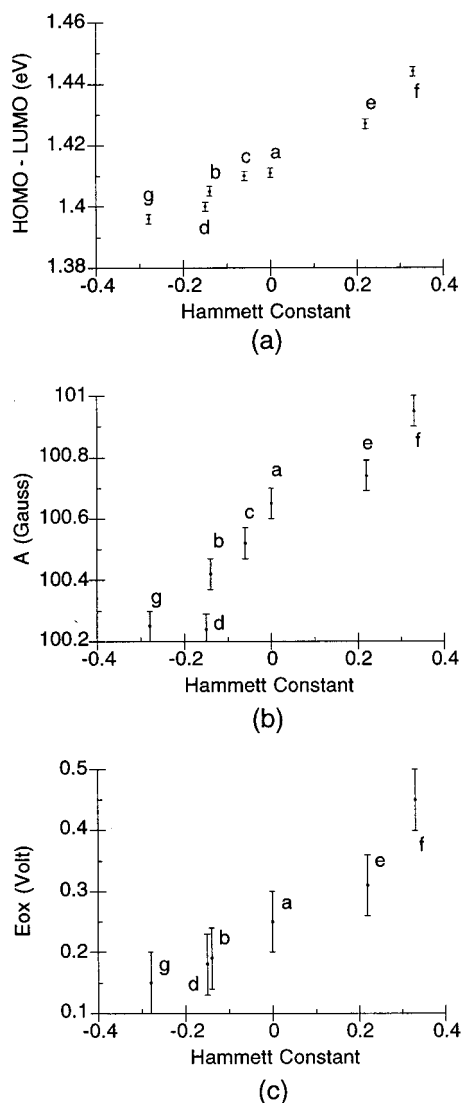


Figure 5. Plots for HOMO–LUMO transitions (a), hyperfine constants (b), and oxidation potentials (c) of $[\text{V}(\text{O})(\text{OR})_2]$ against the Hammett σ constants of the meta and para substituents. (See Figure 1 for substituent patterns.)

atom is located in the plane of N2, C12, and O2,²⁴ which is confirmed by the sum of the bond angles around H1 (359.97°). However, this three-centered bonding mode is not symmetrical. The difference between the combined van der Waals radii and the observed bond lengths is larger for H1–O2 (–0.85 Å) than for H1–C12 (–0.44 Å), and the hydrogen bond to the oxygen atom can therefore be considered to be stronger.

Variable-temperature and deuterium-exchange infrared spectroscopic studies on **2** were carried out to unravel the complex X–H stretching pattern in the region 3100–2800 cm^{-1} , with focus on the intramolecular three-centered hydrogen bonding. In the solid state at ambient temperature (296 K, Fluorolube mull), the H-bond stretching vibration is assigned to the absorption at 2857 cm^{-1} . Upon cooling, a slight blue shift (2859 cm^{-1} at 189 K and 2862 cm^{-1} at 90 K) and an increase in relative intensity are visible. When **2** was prepared from the deuterated phenol (OD), the composite N–D stretching band with a maximum at 2218 cm^{-1} showed a similar sensitivity, viz. blue-shifting and intensity increase upon cooling. The

Table 3. d–d Transition Frequencies^a for **1a–i** in Toluene

no.	complex	assignment			
		$d_{xy} \rightarrow d_{z^2}$	$d_{xy} \rightarrow d_{x^2-y^2}$	$d_{xy} \rightarrow d_{xz}$	$d_{xy} \rightarrow d_{yz}$
1a	H	397	541	≈600	877
1b	4-Me	399	539	≈600	880
1c	5-Me	397	541	≈600	877
1d	4- <i>t</i> -Bu	397	539	≈600	883
1e	4-Cl	396	540	≈600	867
1f	4-N=NPh	<i>b</i>	<i>b</i>	≈600	856
1g	4-OMe	≈400	538	≈600	886
1h^c	4,6-Me ₂	≈400	540	≈600	884
1i^c	4-Me-6-CH ₂ Me ₂	≈400	542	≈600	885

^a Frequency in nanometers; estimated error ± 1 nm. ^b Not observed. ^c In hexane.

complexity of this band can be explained by Fermi resonance between ν_{ND} and $\nu_{\text{CN}}/\nu_{\text{CO}}$ and low-frequency H-bond vibrations. These phenomena as well as the isotope ratio, $\nu_{\text{NH}}/\nu_{\text{ND}} = 1.29$, are in agreement with previously reported vibrational criteria for hydrogen bonding in ortho Mannich bases.^{25,26} However, the X–H stretching frequency of hydrogen-bonded atoms generally shows a red shift upon cooling. This is mainly caused by the decrease in H-bond distance, which results in strengthening of the hydrogen bond. The observed small blue shift of $\nu_{\text{X-H}}$ is most likely due to temperature-induced packing effects, as no changes are expected for the H-bonded proton in **2** because it is sterically shielded.

UV–Vis, EPR, and Redox Behavior. All vanadyl bis-(phenolates), except **1f**, which is red, are dark blue/purple compounds. UV–vis spectra of solutions of compounds **1a–i** in hexane or toluene (Table 3) showed a broad absorption band at approximately 870 nm. According to the molecular orbital scheme for $[\text{VO}(\text{H}_2\text{O})_5]^{2+}$, this transition can be ascribed to the promotion of the single electron from the d_{xy} orbital to the d_{yz} or d_{xz} orbital.²⁷ Valek et al. showed that this degeneracy is lifted in less symmetrical complexes with the d_{yz} orbital being lower in energy.²⁸ The $d_{xy} \rightarrow d_{xz}$ transition at approximately 600 nm is not well-resolved but is visible as a shoulder on the $d_{xy} \rightarrow d_{x^2-y^2}$ transition at 540 nm. However, when the UV–vis spectrum of **1d** was measured in 2-propanol, the two transitions were completely separated. Also the $d_{xy} \rightarrow d_{yz}$ transition is lowered in energy by approximately 50 nm. This difference is caused by the hydrogen-bridge formation between 2-propanol and the $\text{V}=\text{O}$ moiety.²⁹ The $d_{xy} \rightarrow d_{z^2}$ transition appears around 397 nm but is not visible for **1g–i**. In these cases this transition appears as a shoulder on the absorption at approximately 250 nm. This absorption and the one around 200 nm both have high extinction coefficients ($\epsilon > 10\,000 \text{ M}^{-1} \text{ cm}^{-1}$) and are probably due to LMCT or $\pi \rightarrow \pi^*$ transitions.

EPR spectra of these compounds in solution at room temperature showed the expected characteristic octet structure due to hyperfine interaction between the vanadium nucleus ($I = 7/2$) and the unpaired electron. No hyperfine interaction of the nitrogens is resolved. This is due to the small hyperfine constant of a nitrogen nucleus (estimated to be about 2.8 G)³⁰

(25) Rutkowski, K.; Melikova, S. M.; Koll, A. *Vib. Spectrosc.* **1994**, *7*, 265.

(26) Filarowski, A.; Koll, A.; Glowiak, T. *J. Chem. Crystallogr.* **1997**, *27*, 707.

(27) Ballhausen, C. J.; Gray, H. B. *Inorg. Chem.* **1962**, *1*, 111.

(28) Valek, M. H.; Yeranov, W. A.; Basu, G.; Hon, P. K.; Belford, R. L. *J. Mol. Spectrosc.* **1971**, *37*, 228.

(29) Boucher, L. J.; Tynan, E. C.; Yen, T. F. In *Electron Spin Resonance of Metal Complexes*; Yen, T. F., Ed.; Adam Hilger Ltd.: London, 1969; p 111.

(30) Assour, J. M. *J. Chem. Phys.* **1965**, *43*, 2477.

(24) Jeffrey, G. A. *An Introduction to Hydrogen Bonding*; Oxford University Press: New York, 1997; p 22.

Table 4. EPR and Electrochemical Data for **1a–i** and Hammett σ Constants for Substituents **a–g**

complex		EPR ^a			$E_{\text{ox}},^d$
no.	<i>n</i> -R	$\sigma_{\text{m,p}}$	$A_{\text{iso}}, \text{G}^b$	g_{iso}^c	
1a	H	0.00	100.65	1.9719	0.25
1b	4-Me	-0.14	100.42	1.9714	0.19
1c	5-Me	-0.06	100.52	1.9722	
1d	4- <i>t</i> -Bu	-0.15	100.24	1.9717	0.18
1e	4-Cl	0.22	100.74	1.9720	0.31
1f	4-N=NPh	0.33	100.95	1.9720	0.45 ^f
1g	4-OMe	-0.28	100.25	1.9714	0.15
1h	4,6-Me ₂		-100.8 ^e	1.9722 ^e	
1i	4-Me-6-CH ₂ Me ₂		100.5 ^e	1.9722 ^e	

^a In toluene at room temperature. ^b $1 \text{ G} = 0.932 \times 10^{-4} \text{ cm}^{-1}$; estimated error $\pm 0.05 \text{ G}$. ^c Estimated error ± 0.0001 . ^d Potentials referred to a Ag/AgNO₃ electrode in MeCN with Bu₄NPF₆ as supporting electrolyte; estimated error $\pm 0.05 \text{ V}$. ^e In hexane. ^f Poorly resolved.

compared to the line widths, which vary between approximately 10 and 20 G. The line widths are determined by the spin relaxation due to rapid molecular tumbling in solution. Additional line broadening due to spin–spin interactions with neighboring paramagnetic complexes is negligible, as a 100-fold reduction in concentration does not affect the observed line width of the complexes. For complexes with large substituents, such as **1d** and **1f**, the line widths are larger, indicating either larger anisotropy in the hyperfine interaction or slower tumbling of the molecules in solution. We attribute the increase in line widths to the slower tumbling because of the increase of molecular volume caused by the bulkier substituents in these compounds. An increase in molecular volume is associated with slower tumbling of the molecules.³¹

Analysis of the EPR spectra allows accurate determination of the isotropic hyperfine coupling constant A_{iso} , which is defined as the average of the hyperfine coupling tensors over all orientations of the molecule ($A_{\text{iso}} = \frac{1}{3}(A_{xx} + A_{yy} + A_{zz})$). In a first approximation, it is given by the splitting between successive lines in the EPR spectrum. In practice, the lines are not equally spaced, with splittings typically ranging between 90 and 110 G, and second-order perturbation theory³² is required to extract the values of the g_{iso} factor and A_{iso} . From the experimental spectra, the widths and line positions are taken and fitted (see Table 4). The sign of A_{iso} cannot be determined from the spectra.

The anisotropies of the magnetic tensors provide a sensitive probe for changes in the molecular geometry. Since the presence of the noncoordinating substituents on the ring is expected to have no or little influence on the molecular geometry, comparison of the magnetic tensors of complexes **1a–h** with those of **1i** would allow determination of the bonding mode of ligand **i** in complex **1i**. When **i** is present as a bidentate ligand, complex **1i** will have the same geometry as the other complexes (**1a–h**). To obtain this information, frozen-solution spectra have to be measured. Under these conditions, the spectral line shape takes the form of a powder spectrum from which the individual eigenvalues of the magnetic tensors, rather than their isotropic averages, can be extracted by spectral simulation. The EPR spectra of **1d** and **1i** were measured in frozen 2-propanol at 140 K. The EPR spectra are approximately 1000 G wide and appear as powder spectra of compounds with clearly resolved anisotropies in the magnetic interactions. The spectra are dominated by the strong absolute values and anisotropies of

Table 5. Anisotropic *A* and *g* Values for **1d** and **1i**^a

complex									
no.	<i>n</i> -R	A_{xx}	A_{yy}	A_{zz}	A_{iso}	g_{xx}	g_{yy}	g_{zz}	g_{iso}
1d	4- <i>t</i> -Bu	60	60	180	100	1.974	1.982	1.949	1.968
1i	4-Me-6-CH ₂ Me ₂	60.5	60	180	100.2	1.972	1.982	1.947	1.967

^a In 2-propanol at 140 K. *A* values in gauss; estimated error $\pm 1 \text{ G}$. Estimated error in *g* ± 0.001 .

the **A** hyperfine tensor of the vanadium nucleus. On top of this, a relatively small effect of the anisotropy of the **g** tensor is observed, since the spectra are not symmetric. By means of spectral simulation,³³ the anisotropic *A* and *g* values were obtained (see Table 5). The calculated isotropic *A* and *g* values differ only slightly from the measured values, and this means no structural changes have occurred during freezing. The observed differences can be attributed to solvent effects. The *x* and *y* components of the **A** and **g** tensors are approximately equal, indicating an axial symmetry for these complexes. Since g_{zz} is smaller than g_{iso} , it can be concluded that the unpaired electron is located in the d_{xy} orbital,³⁴ as was already concluded from the UV–vis analyses. The location of the unpaired electron in the d_{xy} orbital is confirmed by molecular modeling. ZINDO configuration interaction calculations on the X-ray structure of **1a** showed the HOMO to be a nonbonding orbital with mainly *d* character situated between the V–O and V–N bonds with the V=O bond as the symmetry axis. The *d*–*d* transitions from this orbital were calculated at 937, 538, 480, and 387 nm, respectively. These predictions are in reasonable agreement with experimental values (see Table 3).

Since the anisotropic *A* and *g* values of both complexes **1d** and **1i** are approximately equal, it is clear that both complexes have the same geometry. This means the ligands in complex **1i** are bonded in a bidentate fashion and both second amine functions are just present as ortho-hindering substituents. However, this hindering does not lead to a further distortion of the geometry toward a trigonal bipyramidal structure (vide supra), since this would be observed by a change in A_{xx} .³⁵

Electrochemical measurements on complexes **1a,b,d–g** were carried out in MeCN with Bu₄NPF₆ as supporting electrolyte. The values were measured against Ag/AgNO₃ (see Table 4). A single oxidation step from vanadium(IV) to vanadium(V) was visible at potentials varying between 0.15 and 0.45 V.³⁶ However, upon repetition of the measurements, the oxidation step became increasingly more difficult to observe because of the buildup of other redox-active species. Apparently, the formed vanadium(V) compound is not stable and is immediately reduced to another redox-active species. This reduction is caused by the amine function present in the molecule and is also observed in the attempted synthesis of vanadium(V) complexes of **h**.³⁷ In agreement with these findings, no reduction step of vanadium(V) to vanadium(IV) is visible.

In MeCN, no reduction of the vanadium(IV) compounds to vanadium(III) compounds was observed by cyclic voltammetry.

Influence of Ligand Substituents. For the complexes with electron-withdrawing substituents **1e** and **1f**, an increase in hyperfine constant, oxidation potential, and $d_{xy} \rightarrow d_{yz}$ transition

(31) Henrici-Olivé, G.; Olivé, S. *J. Am. Chem. Soc.* **1971**, *93*, 4154.

(32) Atherton, N. *Electron Spin Resonance*; Wiley: New York, 1973; Section 3.12.

(33) Spectral simulations were carried out using the Bruker WINEPR SymFonia program.

(34) Zah-Letho, J.; Samuel, E.; Livage, J. *Inorg. Chem.* **1988**, *27*, 2233.

(35) Cornman, C. R.; Geiser-Bush, K. M.; Rowley, S. P.; Boyle, P. D. *Inorg. Chem.* **1997**, *36*, 6401.

(36) Oxidation potentials were determined at the top of the oxidation step. Although the absolute oxidation potential cannot be determined for irreversible oxidations, the relative values are reliable.

(37) Hagen, H.; et al. To be published.

occurs compared to the case of **1a**. For the complexes with electron-donating substituents **1b–1e** and **1g**, the opposite is true. To discover the relation between meta and para substitution and the effect on the vanadium nucleus, the energies for the $d_{xy} \rightarrow d_{yz}$ transition, the hyperfine couplings, and the oxidation potentials were plotted against the value for the electronic influence of substituents, the Hammett constant σ (see Figure 5).

All three plots show a reasonable linear relation, and statistical analysis gives the following relations to describe the dependence on σ :

$$\text{UV-vis: } E \text{ (eV)} = 1.41 + 0.08\sigma \quad (1)$$

$$\text{EPR: } A \text{ (G)} = 100.55 + 1.15\sigma \quad (2)$$

$$\text{CV: } E_{\text{ox}} \text{ (V)} = 0.24 + 0.33\sigma \quad (3)$$

The correlations have reasonable r values of 0.98, 0.95, and 0.99,³⁸ respectively, and they show similar trends with significant differences. Thus, with rather small adjustments in the phenoxy ligand system, the electronic properties of the bound vanadium(IV) nucleus can be varied over a large range ($\Delta E_{\text{ox}} = 300$ mV). The dependence of the oxidation potential on the substituent ($dE_{\text{ox}}/d\sigma = 170$ mV (per phenoxy ligand)) is higher than that found for the nickel aryl catalyst system $[\text{Ni}(\text{C}_6\text{H}_2(\text{CH}_2\text{Me}_2)_2\text{-2,6-R-4})\text{Br}]$ ($dE_{\text{ox}}/d\sigma = 120$ mV), which has previously

(38) For this fit, the value for **1f** has been left out because this value could not be determined accurately. If it had been taken into account, the equation would have been $E_{\text{ox}} = 0.26 + 0.45\sigma$; $r = 0.96$.

(39) van de Kuil, L. A.; Luitjes, H.; Grove, D. M.; Zwikker, J. W.; van der Linden, J. G. M.; Roelofsen, A. M.; Jenneskens, L. W.; Drenth, W.; van Koten, G. *Organometallics* **1994**, *13*, 468.

been studied in our group.³⁹ Although it is difficult to conclude whether this difference between the present vanadium(IV) system and the Ni(II) system is due to the monoanionic ligand system, i.e. O vs C anion, or the nature of the metal center or both, it is obvious that extensive electronic communication via the oxygen to vanadium can be achieved. The range wherein the electronic properties can be varied can be extended, since stronger electron-donating and -withdrawing substituents are available, e.g. NMe₂ and CN. This makes these ligands powerful tools for tuning catalytic activity.

Another interesting feature is that, since three independent linear relations have been found, it is possible to use either the hyperfine coupling constant or the HOMO–LUMO transition to predict the oxidation potential. This may be of great use since determination of the oxidation potentials for complexes with strong electron-withdrawing groups might give rise to problems (vide supra).

Studies of the catalytic activity of related complexes in ethene polymerization reactions are in progress.

Acknowledgment. This work was carried out in connection with NIOK, The Netherlands Institute for Catalysis Research, and supported by the Department of Economic Affairs of The Netherlands.

Supporting Information Available: Supporting Information Available: A thermal gravimetry analysis (TGA) plot for **2**, an EPR spectrum of **1a** in hexane at room temperature, measured and simulated EPR spectra of **1d** and **1i** in 2-propanol at 140 K, a CV plot for **1a**, and two crystallographic files in CIF format. This material is available free of charge via the Internet at <http://pubs.acs.org>.

IC9901564